Linking vegetation to climate using ecosystem pressure-volume relationships

Oliver Binks: CREAF, Cerdanyola del Vallès, Barcelona, Spain; ojbinks@gmail.com

Patrick Meir: School of Geosciences, University of Edinburgh, EH9 3FF, United Kingdom; pwmeir@gmail.com

Alexandra G. Konings: Stanford University, Stanford, CA, USA; konings@stanford.edu

Lucas Cernusak: College of Science and Engineering, James Cook University, Cairns, Qld 4878, Australia; lucas.cernusak@jcu.edu.au

Bradley O. Christoffersen: University of Texas Rio Grande Valley, Edinburg, USA; bradley.christoffersen@utrgv.edu

William R. L. Anderegg: School of Biological Sciences, University of Utah, Salt Lake City, Utah, USA; Wilkes Center for Climate Science and Policy, University of Utah, Salt Lake City, Utah, USA; anderegg@utah.edu

Jeffrey Wood: University of Missouri, Columbia, Missouri, USA; woodjd@missouri.edu

Lawren Sack: University of California, Los Angeles, CA, USA; lawrensack@gmail.com

Jordi Martinez-Vilalta: CREAF, Cerdanyola del Vallès, Barcelona, Spain; Universitat Autònoma de Barcelona, Barcelona, Spain; Jordi.Martinez.Vilalta@uab.cat

Maurizio Mencuccini: CREAF, Cerdanyola del Vallès, Barcelona, Spain; Institució Catalana de Recerca i Estudis Avançats (ICREA), Barcelona, Spain; m.mencuccini@creaf.uab.cat

Statement of authorship: OB initially conceived the idea for this work, generated the models, analysed the data, and wrote the manuscript. PM, AGK, LC, BOC, WRLA, JW, LS, JMV,

and MM all contributed substantially to developing the concepts, refining the ideas and successive improvements in the manuscript.

Data accessibility statement: Data will be made available on acceptance of the article.

Running Title: The Ecosystem Pressure-Volume Curve

Key words: Ecosystem function, tree hydraulics, moisture release curves, forest water content, ecosystem water potential, ecohydrological equilibrium theory

Article Type: Perspective

Word count: Abstract – 200; Main text – 6389; text boxes – 795, total – 7184

Number of references: 105

Number of figures: Figures – 6; Tables – 1; Text boxes – 3

*Corresponding author***:** Oliver Binks, OJBinks@gmail.com, Orcid – 0000-0002-6291-3644

Abstract – 200 words max

The relationships between water potential and water content in plants and soil have long been of interest, and there is increasing focus on understanding how these fundamental measures are linked at larger spatial and temporal scales. In this *Perspective*, we explore how the theory of pressure-volume (PV) relationships can be applied at ecosystem scale. We define and evaluate the concept and limitations of the ecosystem and vegetation pressure-volume curves and discuss its application using existing data. As a proof of concept, plot-scale aboveground vegetation PV curves were generated from equilibrium (e.g. predawn) water potentials and water content of the above ground biomass of nine plots including tropical rainforest, savanna, temperate forest, and a long-term Amazonian rainforest drought experiment. Initial findings suggest high consistency among sites where the steady-state water:biomass ratio is approximately 1:3, while the relative values of ecosystem hydraulic capacitance and accessible water storage (the water volume between saturation and a threshold) do not vary systematically with biomass. The ecosystem-scale PV relationship provides a thermodynamically consistent steady-state view of ecosystem form and function and a biophysically robust basis for the interpretation of remote sensing data of vegetation and soil water content, with promise for revealing useful trends across ecosystems.

Introduction

Water fluxes from the land surface to the atmosphere deplete pools of water stored in vegetation and soil. These fluxes are mediated by water potential (Ψ), a thermodynamic property relating to the driving force for the movement of water in the environment. Water potential directly determines hydraulic conductivity in both soil (van Genuchten 1980) and plants. In the latter, water potential is a central physiological variable characterising water status and mediating stomatal conductance (Brodribb & Holbrook 2003; Henry *et al.* 2019), hydraulic conductance, and mortality thresholds associated with water stress (Tyree & Sperry 1989; McDowell *et al.* 2022). Characterising the feedbacks between stores and fluxes of water requires relating water content (θ) to Ψ – subsequently referred to as pressure-volume curves (PV curves) for both soil and plants. While PV curves tend to be carried out on small samples (i.e., leaves, stems, or ex-situ soil samples), there is mounting interest in understanding how these fundamental measures of water are linked at larger spatial scales (Konings *et al.* 2021). The relationship between water potential and water volume at landscape-scale may shed novel insights into ecosystem function (Martinez-Vilalta *et al.* 2019; Wood *et al.* 2023), and facilitate the interpretation of remote sensing data (Konings *et al.* 2021). The conceptual ecosystem-level PV curve (EPV) introduced here represents an effort to reconcile our detailed understanding of biophysical processes at sample-scale, with the scale at which land surface models operate, and at which tower-based, airborne and satellite remote sensing can provide information.

In pressure-volume curves, water volume is typically expressed as an intensive variable (a property whose magnitude is independent of the size of the system, **Box 1**), either per volume of medium (plant tissue, soil), or relative to a maximum value. Both Ψ and θ being intensive, the PV relationship is scale invariant where the implicit assumption is that the medium is structurally/biologically homogeneous. Applying it at larger scales, however, inevitably

includes varying proportions of media with distinct PV relationships. In this respect, the volume (an extensive property) and specific part of the system of interest influence the emergent PV relationship. Moreover, linking fluxes, the exchange of absolute quantities, to pressure-volume states requires an understanding of the total volume of water in the system, i.e., linking intensive with extensive properties. All else equal, a higher volume system will have a smaller change in water potential per unit water loss: a higher hydraulic capacitance. Thus, here we distinguish the intensive variable 'water content' θ, which can be applied to any part of the system, from the extensive volume of stored water, *S*, in a system of volume, *V*, where $S = \theta \cdot V$. While we seldom refer to ecosystem volume directly, global distributions of biomass, *B*, have been well characterised (Spawn *et al.* 2020; Ma *et al.* 2021), where $B = \bar{\rho} \cdot V$ and $\bar{\rho}$ is mean wood density. Consequently, biomass, water volume and water potential of ecosystems are fundamentally linked and determine the feedbacks between vegetation and climate.

Understanding the links between water volume, water potential, biomass and climate may provide key insights into ecosystem function and community assembly at large scales (Lin 2015). Bridging the gap between tissue-level physiological variables and ecosystem-level processes creates the potential for identifying large-scale vegetation thresholds (Hartmann *et al.* 2018) while generating a biophysically robust basis for interpreting remote sensing data (Konings *et al.* 2019). Increased capability for ecosystem monitoring also improves the capacity to model vegetation responses to climate variability, and provides the potential for identifying early warning signals of ecosystem change (Anderegg *et al.* 2019).

The concept that plant communities tend towards steady-states of equilibrium water potential (Box 2) and biomass is consistent with predictable biogeographical patterns in global biome distribution (Humboldt & Bonpland 1805; Holdridge 1947). Several theories take a probabilistic approach to ecosystem organisation, including Eagleson's ecohydrological

equilibrium theory (Eagleson 1982) and maximum entropy production theory (Kleidon & Schymanski 2008; Kleidon *et al.* 2010), in both of which, ecosystems are proposed to converge on optimal solutions with respect to community-level properties (e.g., biomass, water storage, leaf area index). Indeed, multiple plant- to stand-scale vegetation models use steady-state traits to predict longer-term vegetation responses (Cabon *et al.* 2018; Yang *et al.* 2018; Sperry *et al.* 2019) over, e.g. decadal timescales; thereby reducing the need to model sub-daily vegetation-climate feedbacks. Thus, a complementary approach to modelling fluxes in process-based models could be to model steady-states of ecosystem water potential (Ψ_E) and water volume (S_E) in response to the longer-term average conditions, i.e., a 'state-based' modelling approach, relating to the thermodynamic concept of a state function. Potential advantages of a state-based approach include lower data requirements, sharper thresholds for system change (Martinez-Vilalta *et al.* 2019), and the potential to incorporate longer-term vegetation responses such as acclimation in biochemical processes, adaptation in resource allocation, and changes in allometry.

Understanding S_E is also central to the use of microwave and other (e.g. hyperspectral) remote sensing data as a tool for monitoring ecosystem function. Microwave remote sensing measures the dielectric constant of the land surface, which is principally determined by the water contained in biomass, and yields a parameter known as vegetation optical depth (VOD) (Jackson & Schmugge 1991; Konings *et al.* 2016). However, the interpretation of VOD is currently hampered by a lack of information on the amount of water contained in vegetation, and how vegetation water content links to water potential at ecosystem-scale (Konings *et al.* 2021). The potential for using VOD to monitor ecosystem function and health, therefore, requires understanding ecosystem-level relationships between S_E and Ψ_E.

This paper will describe the concept of the ecosystem pressure-volume curve and its possible applications, theoretical and practical. While the PV curve has been applied to many

129 different media, ecosystems differ notably in scale, spatial heterogeneity, and temporal
130 variability. Therefore, we will open the discussion on the applicability of the PV curve to the
131 ecosystem, referring to fundamental physical concepts described more fully in text boxes.
132 We review the theoretical basis for deriving a single value for ecosystem water potential and
133 water volume, together with practical aspects pertaining to measurement in the field and use
134 of existing data. We also estimate what ecosystem and vegetation PV curves may look like,
135 and derive some preliminary conclusions, based on established theory and existing data.

136

137 **Pressure-volume theory and application**

138 Water potential is a measure of free energy, or chemical potential energy, of water and as
139 such the relationship between water potential and water content is of interest in a variety of
140 contexts and media, e.g., leaves (Tyree & Hammel 1972), wood (Meinzer *et al.* 2003), rocks
141 (Franzen & Mirwald 2004), soil (Brooks & Corey 1964), even food (Andrade P *et al.* 2011) –
142 see **Box 3** for a Summary of Water Potential in the Environment. The product of water
143 potential and volume (here $\Psi \cdot \mathcal{S}$) represents the difference in the potential energy available to
144 perform work from the same volume of pure water (Gibbs 1906). In all contexts PV curves
145 have been applied under equilibrium conditions, i.e., the absence of gradients in water
146 potential, and the point to which a system tends given no further exchange of energy or mass
147 (**Box 2**). However, if an ecosystem were to achieve a perfect equilibrium state, Ψ_E would be
148 close to zero at every point within the vertical profile (differing only by gravitation potential)
149 and horizontally across the land surface. This would occur due to capillary rise and vapour
150 transport of water (Rao & Rekapalli 2020) from the water table and horizontal redistribution
151 throughout the soil profile, resulting in full hydration of the plant community. In reality,
152 under conditions of limiting moisture availability, low soil hydraulic conductance prevents

153 the efficient redistribution of water at sub-seasonal timescales leading to gradients of Ψ
154 through the soil profile and, therefore, non-saturated ecosystems by definition cannot be at
155 equilibrium.

156 It is consequently necessary to establish the limitations and boundaries of applying PV theory
157 to non-equilibrium systems. During periods of high flux, systems are further away from
158 equilibrium, have more extreme gradients in water potential, and are more dynamic.
159 Characterising Ψ and θ throughout the system during periods of transpiration requires
160 considerable understanding of the interaction between vegetation physiology, soil properties
161 and the hydraulic environment, thereby having greater data requirements than characterising
162 the system at low to zero flux. The consideration of vertical scale in vegetation is similar to
163 the use of single- versus multi-layer models for vegetation-atmosphere coupling (Raupach &
164 Finnigan 1988). However, in generating ecosystem pressure-volume curves it is also
165 necessary to consider the horizontal spatial variability between species and individuals.

166

167 **Defining ecosystem water potential, Ψ_E**

168 One necessary initial step is to establish the extent of the system, specifically: how deep is an
169 ecosystem? The water table is hydraulically continuous with water in the upper layers of soil
170 and vegetation (Rao & Rekapalli 2020), and the hydraulic conditions below the water table
171 are characterised by the presence of free water ($\Psi \geq 0$ according to depth) across all
172 ecosystems. Ecosystems, therefore, become hydraulically distinct from the water table
173 upwards, making the water table a useful reference point (Binks *et al.* 2021).

174 The challenge of representing a system out of hydraulic equilibrium is in characterising the
175 distribution of both water potential and content, which may vary significantly over small
176 temporal and spatial scales, especially during periods of high flux (**Fig. 1**, Christoffersen et

al. 2016). Assuming comprehensive knowledge of the system, one approach might be to volumetrically weight Ψ between the canopy and water table. Yet, as almost all ecosystem water is contained in the soil (**Fig. 1**e), this would weight Ψ in favour of the part of the system that is least dynamic and least representative of plant water stress. Further, because the relationship between Ψ and θ can be strongly non-linear, Jensen's Inequality applies, where the mean of function(x) is not equal to the function of mean(x) (Ruel & Ayres 1999); as a result, the volume weighted mean water potential is not equal to the equilibrium water potential (SI 1. *A comparison of equilibrium water potential*).

Although a moisture-limited ecosystem is not at equilibrium, non-transpiring plants can theoretically approach hydraulic equilibrium under any prevailing conditions (e.g. **Fig. 1**a and c), either through equilibration with the soil or hydraulic discontinuity between the soil and the roots (Faiz & Weatherley 1982; Rodriguez-Dominguez & Brodribb 2020). In fact, vegetation tends towards a state of hydraulic equilibrium ($\Psi_{V,e}$, where subscript 'e' denotes equilibrium) at night in the absence of nocturnal transpiration (Donovan *et al.* 2003), and during drought when transpiration is minimal (Martínez-vilalta & Garcia-Forner 2017). However, soil water potential gradients result in different 'equilibrium' water potentials between adjacent trees and species arising from varying rooting depths (Sanchez-Martinez *et al.* 2020) leading to horizontal spatial heterogeneity of equilibrium water potentials. Consequently, the mean equilibrium water potential across multiple trees represents the value between the canopy and some representative community-level rooting depth, or functional rooting depth (Binks *et al.* 2021), i.e. the uppermost soil depth at which a plant is hydraulically equilibrated (Donovan *et al.* 2003). Thus, a horizontal spatial average of equilibrium/predawn water potentials would provide a value of water potential that is reasonably representative of both the above ground biomass, and the average soil depth to which the vegetation is equilibrated, within a topographically homogeneous region (**Fig. 1**).

202 Vegetation equilibrium water potentials may therefore be a suitable proxy for ecosystem
203 water potential, $\Psi_{V\_e} \approx \Psi_E$.

204

205 **Defining ecosystem water volume, S_E**

206 The scaling of water content θ to an extensive volume *S* presents the challenge that θ is a
207 property of the medium, not the system. Therefore, even at water potential equilibrium,
208 adjacent media, e.g. leaves, wood, soil, may have very different values of θ.

209 The amount of water contained in the soil environment (S_{soil}) is around one to three orders of
210 magnitude higher than in vegetation on a ground-area basis (**Fig. 1**e). Consequently, the
211 temporal variation of water stored in the upper fraction of a forest canopy is highly dynamic
212 but of low magnitude; while the amount of water stored in soil layers close to the water table
213 varies over longer time scales and is quantitatively substantial. The total water stored in the
214 ecosystem is therefore highly sensitive to the soil depth included in the calculation, and must
215 be considered carefully with respect to its interpretation of temporal trends and comparisons
216 between sites. The remainder of this section focusses on vegetation water, S_V, while S_{soil} is
217 discussed more fully in section: *Soil depth*.

218 Characterising the equilibrium pressure-volume relationships in a whole tree requires
219 consideration of the roots, heartwood, sapwood, bark and leaves. Heartwood comprises 40 –
220 60% of wood volume in mature trees (Cordero *et al.* 2003; Knapic *et al.* 2006; Čermák *et al.*
221 2007; van der Sande *et al.* 2015), but the current consensus is that it does not contribute
222 substantially to plant hydraulic function (Holbrook Gartner 1995; Venturas *et al.* 2017).
223 From a practical perspective, there are very few data on the contribution of heartwood water,
224 or bark, to transpiration, or long-term water balance, on which robust ecosystem-level
225 estimates could be based.

Roots play a key role in ecosystem hydraulics, substantially mediating the conductance of water between the soil and canopy (Steudle 2000; Sperry *et al.* 2003; Rodriguez-Dominguez & Brodribb 2020), whilst typically having different PV characteristics than either leaves or soil (Aritsara *et al.* 2022; Bartlett *et al.* 2022). However, root structure (including biomass) and function is very difficult to characterise, while root water relations also remain poorly understood.

Sapwood contains a physiologically and quantitatively important store of water (S_{sw}) at ecosystem-level, while water stored in leaves (S_{canopy}) may be small in proportion to S_{sw} but likely contributes significantly to daily transpiration fluxes. Moreover, S_{canopy} may also have a disproportionate effect on the VOD signal from microwave remote sensing applications (Holtzman *et al.* 2021). Therefore, a combination of sapwood and canopy water content may be a useful means of characterising water stored in above ground biomass, S_V.

Soil depth

The volume of water stored in soil is a function of soil depth, $S_{soil}(D_x)$. Selecting a representative soil depth requires consideration of the challenges in characterising gradients in Ψ and θ, representation over time, and the possibility for the comparison between different ecosystems.

Unlike plants, the soil environment only reaches water potential equilibrium at saturation while, at other times, the soil water potential profile ranges from monotonic to highly non-monotonic (convex) (Binks *et al.* 2021). Using the water table as a lower limit to soil depth (D_{wt}) has the advantage that the water potential is known (Ψ_0). However, putting aside the challenges of characterising the gradients, D_{wt} differs over time and differs substantially across sites reducing its suitability for temporal and spatial comparisons. Moreover, in many

systems, $S_{soil}(D_{wt})$ would contain enough water to make the vegetation component very small in comparison.

Notwithstanding the issue of predawn disequilibria (discussed later) the predawn plant water potential represents the Ψ_{soil} at functional rooting depth, D_r. D_r also varies across systems and through time according to water availability. The result is that $S_{soil}(D_r)$ can increase as the system becomes drier and plants acquire water from progressively lower depths. Furthermore, as plants tend to equilibrium with the wettest accessible volume of soil, the soil layers above and below D_r are typically not in water potential equilibrium with the plant, meaning that water potential of the adjacent layers is challenging to characterise.

A further possibility is to omit the soil component, which is effectively equivalent to using the functional rooting depth when the soils are saturated, $S_{soil}(D_0) = 0$. This approach omits the largest store of water in the ecosystem which contributes most to evapotranspiration, but weights the response in favour of vegetation dynamics (S_V). Such an approach reduces the uncertainty associated with characterising the soil component of the system, and can be more comprehensively addressed with existing data. In the following sections we address the theory of the Ecosystem PV curve including the soil component, but then generate a 'Proof of concept' using only the vegetation component, i.e. where $S_{soil}(D_0) = 0$.

Ecosystem pressure-volume curves: Ψ_E vs S_E

Following on from the previous discussion, we may treat the ecosystem as having three relevant components, where the total amount of water stored in the ecosystem (S_E) is partitioned between the leaf area (S_{canopy}), sapwood (S_{sw}), and soil (S_{soil}).

$$S_E = S_{canopy} + S_{sw\_plot} + S_{soil} \quad 1.$$

The water contained in each component is the product of its volume (m^3) and water content ($m^3\ m^{-3}$) as a function of Ψ, which we express per ground area as total water thickness (m):

$$S_{soil} = \rho_{water} \cdot D \cdot \theta_{soil}(\Psi) \quad 2.$$

$$S_{sw\_plot}(\Psi) = \rho_{water}\left(\sum_{tree=}^{n} V_{sw\_tree} \cdot \theta_{sw\_tree}(\Psi) \Big/ A_{plot}\right) \quad 3.$$

$$S_{canopy}(\Psi) = LAI \cdot \theta_{leaf}(\Psi) \quad 4.$$

Where D (m) is soil depth (eqn. 2); V_{sw_tree} (eqn. 5 below) is the volume of sapwood per tree in a plot of area A_{plot} (m^2) with n trees (eqn. 3); LAI ($m^2_{leaf\_area}\ m^{-2}_{ground\_area}$) is the leaf area index, and leaf water content (θ_{leaf}) is expressed per one-sided leaf area ($kg\ m^{-2}$, eqn. 4).

Scaling sapwood water content θ_{sw} to tree-level requires the sapwood volume per tree.

$$V_{sw\_tree} = \frac{F_{sw\_tree} AGB_{tree}}{\rho_{wood\_tree}} = F_{sw\_tree} V_{tree} \quad 5.$$

where the subscript '*tree*' denotes individual tree-level values, AGB is the above ground biomass, ρ_{wood} is wood density, and F_{sw} is the volume fraction of sapwood (see SI 2 for derivation of F_{sw}).

Each of the three compartments have different PV curves determining θ(Ψ). The Van Genuchten equation is commonly used to describe PV curves of soil (Hillel 1977):

$$\theta_{soil}(\Psi_i) = \theta_r + \frac{\theta_s - \theta_r}{[1 + (\alpha|\Psi_i|)^n]^{1-1/n}} \quad 6.$$

Where θ subscripts s and r are saturated and residual water contents ($m^3\ m^{-3}$), and α and n are model coefficients.

Both leaf and sapwood PV curves tend to have a linear region at higher values of Ψ (Tyree & Ewers 1991; Meinzer *et al.* 2003; Scholz *et al.* 2007; Bartlett *et al.* 2012; Carrasco *et al.* 2015; Wolfe & Kursar 2015; Ziemińska *et al.* 2020), then rapidly lose water in a post-threshold phase in which hydraulic capacitance ($d\theta/d\Psi$) declines exponentially towards 0. This relationship can be modelled in two phases ('canopy or sapwood' denoted as 'c/sw'):

$$\theta_{c/sw}(\Psi_i) = \begin{cases} \theta_{c/sw}(\Psi_0) - C_{c/sw}\Psi & \Psi > \Psi_{threshold} \\ \theta_{c/sw}(\Psi_{threshold}) \cdot (\Psi_{threshold}/\Psi) & \Psi < \Psi_{threshold} \end{cases} \quad 7.$$

Where subscripts 0 (zero water potential) and *threshold* indicate the corresponding water potentials, and *C* is the (constant) intensive hydraulic capacitance of the linear proportion of the curve. **Figure 2**a illustrates the shapes of the curves and their parameters. The '$\Psi_{threshold}/\Psi$' term in equation 7 is based on a more general form of equation 3 in Christoffersen et al. 2016 describing the post-threshold part of the leaf PV curve. See SI 4 *Deriving post-threshold capacitance in leaves and sapwood.*

Proof of concept

To demonstrate the expected relationship between Ψ and *S* we derived plot-level pressure-volume curves for the nine sites listed in Table S2 representing tropical rainforest, temperate forest, tropical savanna, and semi-arid savanna. These sites were chosen to represent a broad range of biomass, and climates, and on the basis of available data. **See Table 1** for the descriptions, equations and parameter values for each of the variables in the derivation. Values of θ(Ψ) were generated for each component based on a sequence of Ψ from -10 MPa (Ψ_{min}) to 0 (Ψ_0).

Because of the challenges of including the soil component (S_{soil}) in the ecosystem pressure-volume curves (see *Soil Depth*), we included the contribution of soil to the EPV of one site

307 only (SI 3, Fig. S5). For the other sites, we removed the soil component from equation 1
308 generating PV relationships for the above ground biomass components ($S_V = S_{sw} + S_{canopy}$).
309 This is equivalent to using the functional rooting depth of the saturated system, i.e., the
310 vegetation is in equilibrium with the saturated soil surface. This enabled a consistent
311 approach across ecosystems and better represented seasonal and longer-term variation in
312 biomass water content.

313 *Canopy PV curves*

314 Leaf-level PV curves were generated (equations 4 and 7) from each site largely based on the
315 biome-level parameter values reported in Bartlett et al. (2012) and modelled relationships
316 from Christoffersen et al. (2016). Leaf turgor loss point was used as the threshold value for
317 leaves ($\Psi_{TLP} = \Psi_{threshold}$), marking the transition from the linear to the non-linear phase of the
318 PV relationship (Tyree & Hammel 1972). See Table S3 for leaf water relations parameters.

319

320 *Sapwood PV curves*

321 Sapwood PV curves were generated per tree according to equations 3, 5, and 7, and plot-level
322 values were calculated from the combined properties of all trees (**Fig. 2**) based on forest
323 inventory data from the sites listed in Table S2. The individual tree-level approach enables
324 the incorporation of random variability of parameters between individuals and species; and
325 allows the addition of individual- or species-specific traits (e.g. wood density) resulting in
326 different values of $\theta(\Psi)$.

327 The Ψ_0 value in equation 7 was substituted for Ψ_{max} in the sapwood which is the least
328 negative water potential with respect to tree height (**Table 1**) assuming no foliar water uptake
329 (Binks *et al.* 2019).

Ideally, the threshold water potential in sapwood, $\Psi_{threshold}$, should represent the most negative Ψ from which plants can recover full hydraulic function without growing new/replacement tissue (SI 5. *Choosing a threshold water potential*). For the purpose of this *Perspective*, $\Psi_{threshold}$ at plot-level was based on the plot-level mean of the observed dry season midday water potentials (Ψ_{md}). Critically, when the system is at equilibrium *and* the system has dehydrated to the threshold water potential, it follows that the water potential throughout the entire sapwood is also at the threshold water potential (**Fig. 1**c). Thus, when the system is at $\Psi_{threshold}$, the canopy is experiencing a Ψ that occurs within the 'normal' diurnal range, while the majority of the sapwood is experiencing lower than normal water potentials. Individual trees were allocated a value for $\Psi_{threshold}$ taken from a random normal distribution based on the mean and standard error of reported plot-level Ψ_{md} (Table S3).

Vegetation hydraulic capacitance and water storage

Hydraulic capacitance of the above ground biomass was calculated as the sum of tree-level sapwood capacitance and canopy capacitance in the linear phase of the PV curves (C_V, mm MPa^{-1}):

$$C_V = \left(\frac{\sum_{tree=1}^{n}\left(C_{sw\_tree}V_{sw\_tree}\right)}{A_{plot}}\right) + \mathrm{LAI}\left(\frac{\theta_{leaf}(\Psi_0)\left[1-\Theta_{leaf}(\Psi_{TLP})\right]}{-\Psi_{TLP}}\right) \quad 8.$$

Where $\Theta_{leaf}(\Psi_{TLP})$ is the leaf relative water content at turgor loss point ($\theta_{TLP}/\theta_{Saturated}$, **Table 1).**

'Accessible water' (S_{V_a}, mm) was taken to be the difference in S_V between Ψ_{max} and the (equilibrium) threshold water potential, i.e., the difference in water content in panels A and C in **figure 1**.

$$S_{V\_a} = S_V(\Psi_{max}) - S_V(\Psi_{threshold} + sd) \quad 9.$$

The lower boundary was taken to be $\Psi_{threshold}$ + 1 standard deviation of measured Ψ_{md} (*sd*) to account for the distribution of $\Psi_{threshold}$ of the individual trees, half of which would be less negative than plot mean $\Psi_{threshold}$.

Cross-biome relationships between water volume and water potential

One of the objectives of characterising the ecosystem-level PV curve was to test for the existence of cross-biome relationships, potentially identifying hydraulic constraints on the organisation of ecosystems at large spatial and temporal scales.

The greatest conceptual challenge to constructing the ecosystem pressure-volume curve was defining and characterising the soil fraction of the system. Including the soil fraction down to the dry season functional rooting depth, we found that about 6% of the total water (S_E) was contained in the above ground biomass (S_V) in a tropical rainforest system (Fig. S5). However, the calculation did not account for gradients in soil θ and Ψ, presumably resulting in an inaccurate characterisation of the soil component.

Using the water contained in above ground biomass only (S_V) allowed for a more consistent analysis of equilibrium conditions and an informative comparison across sites. The analysis showed a range of $S_V(\Psi_0)$ from 0.2 mm in semi-arid savanna to 17.0 mm in tropical rainforest (**Fig. 3**). Canopy water (S_{canopy}) ranged from 19.4% to 1.2% of $S_V(\Psi_0)$ in the lowest to highest biomass systems, respectively (**Fig. 4**). All of the traits relating to absolute values of $S_V(\Psi_0)$ (**Fig. 5**a-c) were related to stand biomass, including hydraulic capacitance (P = 0.003), accessible storage (P = 0.009), and total maximum water content (i.e. $S_V(\Psi_0)$, P = 0.001). The ratio of $S_V(\Psi_0)$ to biomass was approximately 1:3 (0.31 +/- 0.06 kg_{water} $kg_{biomass}^{-}$

^{1}, regression slope +/- standard error) across all sites (**Fig. 5**c), supporting our expectation for consistent cross-biome steady-state water:carbon relationships. This relationship was largely driven by sapwood water content, although $\theta_{sw}(\Psi_0)$ was derived from an empirical relationship with wood density (Dlouhá *et al.* 2018) which differed across sites, and the relationship included low biomass sites with proportionally higher S_{canopy}.

The relative vegetation capacitance across ecosystems showed no trend with biomass, and an average value of 0.070 MPa^{-1} (+/- 0.023 standard deviation, sd), suggesting that a 7% loss of water equates to an approximate 1 MPa decline in biomass equilibrium water potential across ecosystems (**Fig. 5**d). According to the thresholds selected in the analysis the relative accessible storage, i,e., the maximum difference in S_V without incurring physiological damage, is around 14.6% +/- 7.3 sd (**Fig. 5**e). This value is within the range of empirically derived values of the relative water loss between saturation and the water potential threshold of leaves (i.e., Ψ_{TLP}, Martinez-Vilalta et al. 2019) and stems (Rosner *et al.* 2019). The high level of scatter in the relative parameters may reflect actual ecophysiological differences across sites and/or limitations in data quality. Challenges of estimating $\Psi_{V,e}$ and S_V are discussed in previous sections, but it is possible that the relative water relations parameters are more tightly coordinated across ecosystems than the 'Proof of concept' indicates.

Temporal and spatial resolution

A limitation of using equilibrium water potentials is that they do not capture short-term variation in water status within the canopy, where water stress can be most severe and which is the point of the system to which the VOD signal from microwave remote sensing is most sensitive.

Quantitatively, the fraction of water contained in canopies is small compared to the water contained in sapwood, particularly in high biomass systems. Across the nine sites in this

study, a complete loss of leaf area would result in a median of < 5% decrease in S_V. Leaf turgor loss point is typically around 80-90% relative water content (Bartlett *et al.* 2012; Martinez-Vilalta *et al.* 2019), suggesting daily variations in S_{canopy} of 10-20% of the thickness of the solid lines in **figures 3 and 4**. In contrast, the contribution of sapwood water content (S_{sw}) to daily transpiration may range from 10–50% (Scholz *et al.* 2011) suggesting that, even under non-equilibrium conditions, changes in S_{sw} may lead to relevant differences in S_v. Estimating short-term variation in S_V would require spatially explicit modelling of the vertical profile of biomass, the capacitance and conductance of the hydraulic pathway, the instantaneous flux rate, and the flux history (to capture emptying and refilling of stored water (Meinzer *et al.* 2003)), i.e., a detailed process-based model. However, as vegetation becomes water stressed it tends towards an equilibrium state (**fig. 1c**) where the differences in predawn and midday water potentials decline (Martínez-vilalta & Garcia-Forner 2017) in response to reduced stomatal/canopy conductance (Zeri *et al.* 2014; Mallick *et al.* 2016). Therefore, while equilibrium water potentials do not capture short-term variation, the state-based approach does capture the net change in water content over daily-monthly timescales providing the potential for estimating equilibrium biomass under given conditions, or the change in biomass over longer periods.

Ecological sampling strategies – species versus landscape – traits and properties

Schrodinger argued that the minimum size of a living cell was determined by the scale at which the behavior of molecules become statistically predictable (Schrodinger 1951). Ecological communities modify the conditions of the land surface creating a climatic envelope to which the species within the community are adapted. The result is that purely taxon-level traits may fail to capture properties inherent to the structure of the community and therefore ecosystem-level feedbacks with the wider environment.

Structurally complex vegetation communities generate microclimates that are substantially different from 'external' conditions. Forest understoreys tend to maintain higher humidity and lower temporal variation in temperature and humidity. An analogous process may be common in the soil, where deeply rooted species lose water to drier soil layers in the upper surface (Oliveira *et al.* 2005; Chitra-Tarak *et al.* 2021) buffering temporal variation in Ψ_{soil} in the dense rooting zone. Therefore, while species-specific traits (e.g. rooting depth, stomatal behaviour) are important, canopy position and plant size (including rooting extent) also play powerful roles in determining water supply and demand, both inter- and intra-specifically.

Leaf water potentials measured in field studies, including those used in our 'Proof of concept', are typically taken from a few common species within a community, and represent extreme conditions (Martínez-Vilalta *et al.* 2021). The emergent ecosystem water potential, however, should represent a median community-level value accounting for vegetation structure as this is more relevant to characterising vegetation behaviour under typical conditions. The consequence of using extreme values is somewhat mitigated in this analysis by using predawn equilibrium values, yet differences between, e.g., overstorey and understorey vegetation, may be significant if they correspond to systematic differences in rooting depth. The same is true of any 'trait' we use to characterise vegetation, e.g., vulnerability thresholds: to understand the community, we need to characterise the distribution of values, rather than focusing on the extremes.

Spatial sampling strategies are more suitable for representing emergent properties, relating more directly to landscape-level feedbacks between vegetation, climate and biogeochemical cycles. While species identity is important for characterising plot-scale ecological dynamics, communities with predictable climatically-determined structural properties arise with little species-level taxonomic similarity, e.g. African and South American tropical rainforest (de Miranda *et al.* 2022). Thus, spatial sampling may reveal trends and commonalities between

447 taxonomically distinct but climatically similar systems, while potentially being more practical
448 for characterising highly biodiverse communities.

449 **Modelling applications**

450 The consistency in derived metrics across sites, e.g. in the steady-state water:biomass ratio
451 and relative capacitance, provides a starting point for addressing the question of whether we
452 can model ecosystems as structures that self-organise to achieve a steady-state with respect to
453 longer term environmental pressures. This approach is complementary but distinct from the
454 process-based approach (Fisher *et al.* 2018) by having lower resolution data requirements,
455 requiring only information on 'states' (Ψ and θ), which are more feasibly sampled and
456 interpolated across larger areas, and reducing the dependence on characterising the highly
457 dynamic flux responses and variation across trees, species, size classes and functional types.
458 Our ability to link climate with large scale trends in vegetation properties will continue to
459 increase with the growth of global databases on plant traits (e.g. Mencuccini et al. 2019) and
460 water potentials (Novick *et al.* 2022), coupled with the increased capacity to estimate water
461 content at large scales (Konings *et al.* 2021). Water is more directly linked to climate and
462 land surface energy budgets than is carbon (Malhi *et al.* 2002; Tesař *et al.* 2007; Bonan
463 2008). Thus, in a process analogous to modelling water levels in a lake, the state-based
464 approach may offer an alternative method for making long-term predictions of climate-
465 related changes in vegetation structure such as biomass, leaf area, and allometry.

466 **Thresholds**

467 A key focus of large-scale vegetation ecology is in predicting and detecting thresholds of
468 water stress that lead to significant mortality events or transitions in vegetation type. In
469 sapwood, the transition between the pre- and post-threshold phases of the PV curve is often
470 apparent from a change in the $d\theta/d\Psi$ gradient caused by the release of water from cavitating

vessels (Tyree & Ewers 1991; Hölttä *et al.* 2009). It is possible that a similar mechanism of water release occurs at large spatial and time scales. Drought leads to the death of living biomass (leaves, branches, whole plants) causing the amount of water contained in the system to decrease rapidly, while both the competition for soil water and the soil-atmosphere hydraulic conductance are reduced, slowing the decline in plant equilibrium water potentials. The ecosystem thus transitions into a phase where the loss of S_V happens more rapidly than the change in Ψ_V, and this continues until there is sufficient water for Ψ_V to be maintained within physiologically tolerable limits in the remaining vegetation.

A central consideration of thresholds at community-level is whether there is an acute transition between the pre- and post-$\Psi_{threshold}$ parts of the EPV curve (Wood *et al.* 2023). For the purpose of the 'Proof of concept', the post-$\Psi_{threshold}$ PV relationship was based on the shape of published PV curves, by simplifying the derivation of Christoffersen et al. (2016a). However, the extent that ecosystems follow the same pattern as plant tissues is unknown, and might only become apparent from large-scale observation and experiments (Mcculloh *et al.* 2014; Meir *et al.* 2015). Evidence from the Caxiuanã long-term throughfall exclusion experiment (CTFE) in Amazonian rainforest in Brazil (Meir *et al.* 2018) suggests that the pre- and post-threshold change in $d\theta/d\Psi$ may be considerable, i.e., the transition from one line to the other in **figure 6**. The CTFE excluded 50% of the throughfall from 1 ha of rainforest continuously since 2002, resulting in elevated mortality and lower biomass (da Costa *et al.* 2010; Yao et al. 2022). The droughted forest now has lower ecosystem water content, while the diurnal range of canopy water potentials remains similar, although slightly more negative, than those in the control (Bittencourt *et al.* 2020). The experimental result is consistent with the theory presented here, that changes in the hydraulic environment result in co-dependent changes in biomass and S_V such that the water:biomass ratio is approximately conserved (**Fig. 5**c).

At community-level, transitions may become gradual due to the averaging-effect between individuals of different species and sizes. This is illustrated in **figure 3** where the Caxiuanã traces have a gradual transition due to the higher standard deviation of the Ψ_{md} data (based on 161 trees from 36 species in the Brazilian Amazon (Bittencourt *et al.* 2020)) than in other sites. On the other hand, soil contains such a high proportion of the water in ecosystems (**Figures 1** and S5), that community-level transitions could be driven by the shape of the soil water release curve (Dexter *et al.* 2012; Asgarzadeh *et al.* 2014; Wood *et al.* 2023). The degree of coordination in PV relationships between vegetation and soil requires further investigation.

Remote sensing

The existence of cross-biome relationships between water relations and biomass enables assumptions to be made concerning total water content of ecosystems and the ecophysiological impact of a change in water content. Vegetation optical depth (VOD) has been used to provide information on both biomass (Mialon *et al.* 2020) and water (Grant *et al.* 2012) in ecosystems, but it cannot fully distinguish between the two properties (Dou *et al.* 2023). Therefore, the evidence suggesting that i) maximum vegetation water content varies predictably with biomass, and that ii) relative accessible water storage does not appear to differ systematically between systems (**Fig. 5**), provide a robust basis for inferring ecosystem water status from remote sensing data. Additional research is needed to account for the varying sensitivity of the remote sensing data to canopy water content across different depth layers (Holtzman *et al.* 2021), and what observation times and other conditions would be most closely related to the equilibrium conditions described in this study.

Other considerations

520 According to our preliminary analysis, the largest store of aboveground water was in the
521 sapwood, where sapwood fraction is possibly the largest source of uncertainty.
522 Quantitatively, heartwood water, which can be 30-220% of dry mass (Hillis 1987), is the
523 largest unaccounted-for pool which could influence estimates of VOD, and therefore the
524 interpretation of RS data (Konings *et al.* 2017). Our comparisons of S_V with biomass
525 effectively assume the heartwood is dry, which is arguably a relevant comparison
526 representing the ratio of ecosystem biomass to 'physiologically active' water. However,
527 including the heartwood fraction of water content within the S_V term would affect our results
528 in the following ways: i) the ecosystem-level water:biomass ratio would increase, making it
529 >1:3; ii) the relative storage fractions would decrease in value, i.e. relative capacitance,
530 relative accessible storage, and relative maximum storage; iii) perhaps most significantly, the
531 relationship between S_V and AGB may change from linear to non-linear.

532 Vegetation predawn water potentials are commonly not in water potential equilibrium with
533 the root water source owing to nocturnal fluxes such as transpiration (Donovan *et al.* 2003;
534 Kangur *et al.* 2021) or foliar water uptake (Kangur *et al.* 2017; Binks *et al.* 2019). The soil
535 profile includes all water potentials between zero (water table or the soil surface following
536 rain) and the most negative value. Therefore, the effect of wrongly assuming plants are in
537 equilibrium with the soil is typically in assuming that they are in equilibrium with a different
538 part of the soil profile. If the nocturnal flux is small, it seems likely that the disequilibrium
539 soil depth is also small (Kangur *et al.* 2017).

540 **Conclusion**

541 The ecosystem scale pressure-volume curve reconciles our detailed and physically rigorous
542 understanding of small-scale field-measureable processes to the spatial scale applicable to
543 ecosystem and climate science. The 'state-based' approach to understanding climate-

544 vegetation feedbacks is based on the principle that ecosystems reach a thermodynamic
545 steady-state with respect to environmental conditions. This assumption allows us to use data
546 with low temporal resolution, thereby determining long-term changes in stores of carbon and
547 water, and becoming less dependent on the measurement of processes with high spatial and
548 temporal variability. Acknowledging the existence of additional constraints (e.g. soil
549 nutrients), we propose that to a first approximation the water content of an ecosystem (and its
550 biomass) is a direct function of the hydraulic environment.

551 We conclude that using the water content of the canopy and above ground sapwood, and
552 water potentials during equilibrium (e.g. predawn, or drought) conditions, are practical
553 options for calculating baseline ecosystem PV parameters. This is based on i) the practicality
554 of applying an equilibrium concept to a non-equilibrium system, ii) the relevance of these
555 parameters in relating large-scale vegetation function to the hydraulic environment, and iii)
556 the availability of existing data. Derivations of both Ψ_E and S_E (or Ψ_V and S_{V_e}) could be
557 improved from our estimates with more comprehensive data on water potential, water content
558 and capacitance at larger scale, and better spatial representation across landscapes.

559 Our first estimates here, for a range of ecosystems, suggest that there appears to be a
560 consistent ratio of 'physiologically active water' to biomass across the examined plots of
561 approximately 1:3. In absolute terms, the water available for reversible changes in S_V, and
562 hydraulic capacitance, also increases with biomass. In relative terms, there were no
563 significant relationships between hydraulic properties and biomass, possibly suggesting these
564 relative values are conserved across ecosystems. Such generalisations across biomes offer
565 the first insight into the utility of the state-based approach for gaining ecophysiologically
566 meaningful interpretations of landscape-scale data, and provide a robust basis for the
567 validation of VOD observations.

Acknowledgements

This work was partially inspired by discussions at the "Sensing Forest Water Dynamics from Space: Towards Predicting the Earth System Response to Droughts" workshop, which was initiated and supported by the W.M. Keck Institute for Space Studies.

EU Horizon 2020 grant 862221 to MM; Catalan science and technology grant, Beatriu de Pinós, BP2021 00224 to OB; ARC grant DP17010409, NERC NE/W006308/1 and Royal Society RSWF\211008 to PM

References

Ambaum, M.H.P. (2020). Accurate, simple equation for saturated vapour pressure over water and ice. *Quarterly Journal of the Royal Meteorological Society*, 146, 4252–4258.

Anderegg, W.R.L., Anderegg, L.D.L. & Huang, C. ying. (2019). Testing early warning metrics for drought-induced tree physiological stress and mortality. *Glob Chang Biol*, 25, 2459–2469.

Andrade P, R.D., Lemus, R.M. & Pérez C, C.E. (2011). Models of sorption isotherms for food: uses and limitations. *Vitae*, 18, 325–334.

Aparecido, L.M.T., Miller, G.R., Cahill, A.T. & Moore, G.W. (2016). Comparison of tree transpiration under wet and dry canopy conditions in a Costa Rican premontane tropical forest. *Hydrol Process*, 5011, 5000–5011.

Aritsara, A.N.A., Wang, S., Li, B.-N., Jiang, X., Qie, Y.-D., Tan, F.-S., *et al.* (2022). Divergent leaf and fine root "pressure–volume relationships" across habitats with varying water availability. *Plant Physiol*, 190, 2246–2259.

590 Asgarzadeh, H., Mosaddeghi, M.R., Dexter, A.R., Mahboubi, A.A. & Neyshabouri, M.R.
591 (2014). Determination of soil available water for plants: Consistency between laboratory
592 and field measurements. *Geoderma*, 226–227, 8–20.

593 Bartlett, M.K., Scoffoni, C. & Sack, L. (2012). The determinants of leaf turgor loss point and
594 prediction of drought tolerance of species and biomes: a global meta-analysis. *Ecol Lett*,
595 15, 393–405.

596 Bartlett, M.K., Sinclair, G., Fontanesi, G., Knipfer, T., Walker, M.A. & McElrone, A.J.
597 (2022). Root pressure–volume curve traits capture rootstock drought tolerance. *Ann Bot*,
598 129, 389–402.

599 Beringer, J., Hutley, L.B., McHugh, I., Arndt, S.K., Campbell, D., Cleugh, H.A., *et al.*
600 (2016). An introduction to the Australian and New Zealand flux tower network -
601 OzFlux. *Biogeosciences*, 13, 5895–5916.

602 Binks, O., Cernusak, L.A., Liddell, M., Bradford, M., Coughlin, I., Carle, H., *et al.* (2021).
603 Forest system hydraulic conductance: partitioning tree and soil components. *New*
604 *Phytologist*, 233, 1667–1681.

605 Binks, O., Meir, P., Rowland, L., da Costa, A.C.L.A.C., Vasconcelos, S.S.S.S., de Oliveira,
606 A.A.R.A.A., *et al.* (2016). Plasticity in leaf-level water relations of tropical rainforest
607 trees in response to experimental drought. *New Phytologist*, 211, 477–488.

608 Binks, O., Mencuccini, M., Rowland, L., da Costa, A.C.L.A.C.L., de Carvalho, C.J.R.C.J.R.,
609 Bittencourt, P., *et al.* (2019). Foliar water uptake in Amazonian trees: Evidence and
610 consequences. *Glob Chang Biol*, 25, 1–13.

611 Bittencourt, P.R.L., Oliveira, R.S., da Costa, A.C.L., Giles, A.L., Coughlin, I., Costa, P.B., *et*
612 *al.* (2020). Amazonia trees have limited capacity to acclimate plant hydraulic properties
613 in response to long-term drought. *Glob Chang Biol*, 26, 3569–3584.

614 Bonan, G.B. (2008). Forests and climate change: forcings, feedbacks, and the climate benefits
615 of forests. *Science (1979)*, 320, 1444–1449.

616 Brodribb, T.J. & Holbrook, N.M. (2003). Stomatal Closure during Leaf Dehydration ,
617 Correlation with Other Leaf Physiological Traits 1. *Plant Physiol*, 132, 2166–2173.

618 Brooks, R.H.H. & Corey, A.T.T. (1964). Hydraulic properties of porous media. *Physics and*
619 *Chemistry of Glasses: European Journal of Glass Science and Technology Part B*, 49,
620 293–296.

621 Cabon, A., Martínez-Vilalta, J., Martínez de Aragón, J., Poyatos, R. & De Cáceres, M.
622 (2018). Applying the eco-hydrological equilibrium hypothesis to model root distribution
623 in water-limited forests. *Ecohydrology*, 11, e2015.

624 Carrasco, L.O., Bucci, S.J., di Francescantonio, D., Lezcano, O.A., Campanello, P.I., Scholz,
625 F.G., *et al.* (2015). Water storage dynamics in the main stem of subtropical tree species
626 differing in wood density, growth rate and life history traits. *Tree Physiol*, 35, 354–365.

627 Čermák, J., Kucera, J., Bauerle, W.L., Phillips, N. & Hinckley, T.M. (2007). Tree water
628 storage and its diurnal dynamics related to sap flow and changes in stem volume in old-
629 growth Douglas-fir trees. *Tree Physiol*, 27, 181–198.

630 Chitra-Tarak, R., Xu, C., Aguilar, S., Anderson-Teixeira, K.J., Chambers, J., Detto, M., *et al.*
631 (2021). Hydraulically-vulnerable trees survive on deep-water access during droughts in
632 a tropical forest. *New Phytologist*, 231, 1798–1813.

633 Christoffersen, B.O., Gloor, M., Fauset, S., Fyllas, N.M., Galbraith, D.R., Baker, T.R., *et al.*
634 (2016a). Linking hydraulic traits to tropical forest function in a size-structured and trait-
635 driven model (TFS v.1-Hydro). *Geosci Model Dev*, 9.

636 Cordero, L.D.P., Kanninen, M., Diego, L., Cordero, P. & Kanninen, M. (2003). Heartwood,
637 sapwood and bark content, and wood dry density of young and mature teak (Tectona
638 grandis) trees grown in Costa Rica. *Silva Fennica*, 37, 45–54.

639 da Costa, A.C.L., Galbraith, D., Almeida, S., Portela, B.T.T., da Costa, M., Silva Junior,
640 J.D.A., *et al.* (2010). Effect of 7 yr of experimental drought on vegetation dynamics and
641 biomass storage of an eastern Amazonian rainforest. *New Phytol*, 187, 579–91.

642 DAAC, O. (2017). MODIS and VIIRS Land Products Global Subsetting and Visualization
643 Tool. *ORNL DAAC*.

644 Dexter, A.R., Czyz, E.A. & Richard, G. (2012). Equilibrium, non-equilibrium and residual
645 water: Consequences for soil water retention. *Geoderma*, 177–178, 63–71.

646 Dlouhá, J., Alméras, T., Beauchêne, J., Clair, B. & Fournier, M. (2018). Biophysical
647 dependences among functional wood traits. *Funct Ecol*, 32, 2652–2665.

648 Donovan, L.A., Richards, J.H. & Linton, M.J. (2003). Magnitude and Mechanisms of
649 Disequilibrium between Predawn Plant and Soil Water Potentials. *Ecology*, 84, 463–
650 470.

651 Dou, Y., Tian, F., Wigneron, J.P., Tagesson, T., Du, J., Brandt, M., *et al.* (2023). Reliability
652 of using vegetation optical depth for estimating decadal and interannual carbon
653 dynamics. *Remote Sens Environ*, 285, 113390.

654 Eagleson, P.$. (1982). Ecological Optimality in Water-Limited Natural Soil-Vegetation
655 Systems 1. Theory and Hypothesis. *Water Resour Res*, 18, 325–340.

656 Faiz, S.M.A. & Weatherley, P.E. (1982). Root Contraction in Transpiring Plants. *New*
657 *Phytologist*, 92, 333–343.

658 Fisher, R. a, Williams, M., Do Vale, R.L., Da Costa, A.L., Meir, P., Lobo Do Vale, R., *et al.*
659 (2006). Evidence from Amazonian forests is consistent with isohydric control of leaf
660 water potential. *Plant Cell Environ*, 29, 151–65.

661 Fisher, R.A., Koven, C.D., Anderegg, W.R.L., Christoffersen, B.O., Dietze, M.C., Farrior,
662 C.E., *et al.* (2018). Vegetation demographics in Earth System Models: A review of
663 progress and priorities. *Glob Chang Biol*, 24, 35–54.

664 Franzen, C. & Mirwald, P.W. (2004). Moisture content of natural stone: Static and dynamic
665 equilibrium with atmospheric humidity. *Environmental Geology*, 46, 391–401.

666 Gartner, B.L. (1995). Plant stems : physiology and functional morphology, 440.

667 van Genuchten, M.Th. (1980). A Closed-form Equation for Predicting the Hydraulic
668 Conductivity of Unsaturated Soils. *Soil Science Society of America Journal*.

669 Gibbs, J.W. (1906). *Scientific Papers of Josiah Willard Gibbs, Volume 1 - Wikisource, the*
670 *free online library*. *Scientific Papers of Josiah Willard Gibbs*. Available at:
671 https://en.wikisource.org/wiki/Scientific_Papers_of_Josiah_Willard_Gibbs,_Volume_1.
672 Last accessed 25 November 2022.

673 *GMDD - Forest fluxes and mortality response to drought: model description (ORCHIDEE-*
674 *CAN-NHA, r7236) and evaluation at the Caxiuanã drought experiment*. (2022). .
675 Available at: https://gmd.copernicus.org/preprints/gmd-2021-362/. Last accessed 12
676 October 2022.

677 Grant, J.P., Wigneron, J.P., Drusch, M., Williams, M., Law, B.E., Novello, N., *et al.* (2012).
678 Investigating temporal variations in vegetation water content derived from SMOS

optical depth. *International Geoscience and Remote Sensing Symposium (IGARSS)*, 3331–3334.

Hartmann, H., Moura, C.F., Anderegg, W.R.L., Ruehr, N.K., Salmon, Y., Allen, C.D., *et al.* (2018). Research frontiers for improving our understanding of drought-induced tree and forest mortality. *New Phytologist*, 218, 15–28.

Henry, C., John, G.P., Pan, R., Bartlett, M.K., Fletcher, L.R., Scoffoni, C., *et al.* (2019). A stomatal safety-efficiency trade-off constrains responses to leaf dehydration. *Nature Communications 2019 10:1*, 10, 1–9.

Hillel, D. (1977). Environmental Soil Physics - 1st Edition. *No. of pages: 771 Language: English Copyright: © Academic Press 1998 Published: 31st August 1998 Imprint: Academic Press Hardcover ISBN: 9780123485250 eBook ISBN: 9780080544151*, 771.

Hillis, W.E. (1987). Heartwood and Tree Exudates. Springer Series in Wood Science, 4.

Holdridge, L.R. (1947). Determination of world plant formations from simple climatic data. *Science (1979)*, 105, 367–368.

Hollander, E.H.D. (1979). Estimation of the Pore Size Distribution From the Moisture Characteristic, 15.

Hölttä, T., Cochard, H., Nikinmaa, E. & Mencuccini, M. (2009). Capacitive effect of cavitation in xylem conduits: Results from a dynamic model. *Plant Cell Environ*, 32, 10–21.

Holtzman, N.M., Anderegg, L.D.L., Kraatz, S., Mavrovic, A., Sonnentag, O., Pappas, C., *et al.* (2021). L-band vegetation optical depth as an indicator of plant water potential in a temperate deciduous forest stand. *Biogeosciences*, 18, 739–753.

Humboldt, A. von & Bonpland, A. (1805). *Essai sur la géographie des plantes : accompagné d'un tableau physique des régions équinoxiales, fondé sur des mesures exécutées, depuis le dixième degré de latitude boréale jusqu'au dixième degré de latitude australe, pendant les années 1799, 1800, 1801, 1802 et 1803*. Chez Levrault, Schoell et compagnie, libraires, A Paris.

Jackson, T.J. & Schmugge, T.J. (1991). Vegetation effects on the microwave emission of soils. *Remote Sens Environ*, 36, 203–212.

Kangur, O., Kupper, P. & Sellin, A. (2017). Predawn disequilibrium between soil and plant water potentials in light of climate trends predicted for northern Europe. *Reg Environ Change*, 17, 2159–2168.

Kangur, O., Steppe, K., Schreel, J.D.M., Von Der Crone, J.S. & Sellin, A. (2021). Variation in nocturnal stomatal conductance and development of predawn disequilibrium between soil and leaf water potentials in nine temperate deciduous tree species. *Functional Plant Biology*, 48, 483–492.

Kleidon, A., Malhi, Y. & Cox, P.M. (2010). Maximum entropy production in environmental and ecological systems. *Philosophical Transactions of the Royal Society B: Biological Sciences*, 365, 1297–1302.

Kleidon, A. & Schymanski, S. (2008). Thermodynamics and optimality of the water budget on land: A review. *Geophys Res Lett*, 35, 1–6.

Knapic, S., Tavares, F. & Pereira, H. (2006). Heartwood and sapwood variation in Acacia melanoxylon R. Br. trees in Portugal. *Forestry*, 79, 371–380.

Konings, A.G., Feng, X., Molini, A., Manzoni, S., Vico, G. & Porporato, A. (2012). Thermodynamics of an idealized hydrologic cycle. *Water Resour Res*, 48, 1–13.

724 Konings, A.G., Piles, M., Rötzer, K., McColl, K.A., Chan, S.K. & Entekhabi, D. (2016).
725 Vegetation optical depth and scattering albedo retrieval using time series of dual-
726 polarized L-band radiometer observations. *Remote Sens Environ*, 172, 178–189.

727 Konings, A.G., Rao, K. & Steele-Dunne, S.C. (2019). Macro to micro: microwave remote
728 sensing of plant water content for physiology and ecology. *New Phytologist*, 223, 1166–
729 1172.

730 Konings, A.G., Saatchi, S.S., Frankenberg, C., Keller, M., Leshyk, V., Anderegg, W.R.L.L.,
731 *et al.* (2021). Detecting forest response to droughts with global observations of
732 vegetation water content. *Glob Chang Biol*, 27, 1–20.

733 Konings, A.G., Yu, Y., Xu, L., Yang, Y., Schimel, D.S. & Saatchi, S.S. (2017). Active
734 microwave observations of diurnal and seasonal variations of canopy water content
735 across the humid African tropical forests. *Geophys Res Lett*, 44, 2290–2299.

736 Kunert, N., Aparecido, L.M.T., Wolff, S., Higuchi, N., Santos, J. dos, Araujo, A.C. de, *et al.*
737 (2017). A revised hydrological model for the Central Amazon: The importance of
738 emergent canopy trees in the forest water budget. *Agric For Meteorol*, 239, 47–57.

739 Lin, H. (2015). Thermodynamic entropy fluxes reflect ecosystem characteristics and
740 succession. *Ecol Modell*, 298, 75–86.

741 Ma, H., Mo, L., Crowther, T.W., Maynard, D.S., van den Hoogen, J., Stocker, B.D., *et al.*
742 (2021). The global distribution and environmental drivers of aboveground versus
743 belowground plant biomass. *Nature Ecology & Evolution 2021 5:8*, 5, 1110–1122.

744 Malhi, Y., Pegoraro, E., Nobre, A.D., Pereira, M.G.P., Grace, J., Culf, A.D., *et al.* (2002).
745 Energy and water dynamics of a central Amazonian rain forest. *Journal of Geophysical*
746 *Research Atmospheres*, 107, 1–17.

747 Martinez-Vilalta, J., Anderegg, W.R.L., Sapes, G. & Sala, A. (2019). Greater focus on water
748 pools may improve our ability to understand and anticipate drought-induced mortality in
749 plants. *New Phytologist*, 223, 22–32.

750 Martínez-vilalta, J. & Garcia-forner, N. (2017). Water potential regulation , stomatal
751 behaviour and hydraulic transport under drought : deconstructing the iso / anisohydric
752 concept, 962–976.

753 Martínez-Vilalta, J., Santiago, L.S., Poyatos, R., Badiella, L., de Cáceres, M., Aranda, I., *et*
754 *al.* (2021). Towards a statistically robust determination of minimum water potential and
755 hydraulic risk in plants. *New Phytologist*, 232, 404–417.

756 Mc Naught, a. D. & Wilkinson, a. (2012). Compendium of Chemical Terminology-Gold
757 Book. *Iupac*, 1670.

758 Mcculloh, K.A., Johnson, D.M., Meinzer, F.C. & Woodruff, D.R. (2014). The dynamic
759 pipeline: hydraulic capacitance and xylem hydraulic safety in four tall conifer species.
760 *Plant Cell Environ*, 37, 1171–83.

761 McDowell, N.G., Sapes, G., Pivovaroff, A., Adams, H.D., Allen, C.D., Anderegg, W.R.L., *et*
762 *al.* (2022). Mechanisms of woody-plant mortality under rising drought, CO2 and vapour
763 pressure deficit. *Nature Reviews Earth & Environment 2022 3:5*, 3, 294–308.

764 Meinzer, F.C., James, S.A., Goldstein, G., Woodruff, & D. & Woodruff, D. (2003). Whole-
765 tree water transport scales with sapwood capacitance in tropical forest canopy trees.
766 *Plant Cell Environ*, 26, 1147–1155.

767 Meir, P., Meir, P., Mencuccini, M. & Dewar, R.C. (2015). Drought-related tree mortality:
768 Addressing the gaps in understanding and prediction. *New Phytologist*, 207, 28–33.

769 Meir, P., Mencuccini, M., Binks, O., Da Costa, A.L., Ferreira, L. & Rowland, L. (2018).
770 Short-term effects of drought on tropical forest do not fully predict impacts of repeated
771 or long-term drought: Gas exchange versus growth. *Philosophical Transactions of the*
772 *Royal Society B: Biological Sciences*, 373.

773 Mencuccini, M., Rosas, T., Rowland, L., Choat, B., Cornelissen, H., Jansen, S., *et al.* (2019).
774 Leaf economics and plant hydraulics drive leaf : wood area ratios. *New Phytologist*, 224,
775 1544–1556.

776 Mialon, A., Rodríguez-Fernández, N.J., Santoro, M., Saatchi, S., Mermoz, S., Bousquet, E.,
777 *et al.* (2020). Evaluation of the Sensitivity of SMOS L-VOD to Forest Above-Ground
778 Biomass at Global Scale. *Remote Sensing 2020, Vol. 12, Page 1450*, 12, 1450.

779 de Miranda, P.L.S., Dexter, K.G., Swaine, M.D., de Oliveira-Filho, A.T., Hardy, O.J. &
780 Fayolle, A. (2022). Dissecting the difference in tree species richness between Africa and
781 South America. *Proc Natl Acad Sci U S A*, 119, e2112336119.

782 Monteith, J. & Unsworth, M. (2013). Principles of Environmental Physics: Plants, Animals,
783 and the Atmosphere: Fourth Edition. *Principles of Environmental Physics: Plants,*
784 *Animals, and the Atmosphere: Fourth Edition*, 1–401.

785 Moore, G.W., Orozco, G., Aparecido, L.M.T. & Miller, G.R. (2017). Upscaling transpiration
786 in diverse forests: Insights from a tropical premontane site. *Ecohydrology*, 11, 1–13.

787 Nobel, P.S. (2009). Physicochemical and Environmental Plant Physiology. *Physicochemical*
788 *and Environmental Plant Physiology*.

789 Novick, K.A., Ficklin, D.L., Baldocchi, D., Davis, K.J., Ghezzehei, T.A., Konings, A.G., *et*
790 *al.* (2022). Confronting the water potential information gap. *Nature Geoscience 2022*
791 *15:3*, 15, 158–164.

792 Oliveira, R.S., Dawson, T.E., Burgess, S.S.O.O. & Nepstad, D.C. (2005). Hydraulic
793 redistribution in three Amazonian trees. *Oecologia*, 145, 354–363.

794 Pickard, W.F. (1981). The ascent of sap in plants. *Prog Biophys Mol Biol*, 37, 181–229.

795 Rao, S.M. & Rekapalli, M. (2020). Identifying the dominant mode of moisture transport
796 during drying of unsaturated soils. *Scientific Reports 2020 10:1*, 10, 1–9.

797 Raupach, M.R. & Finnigan, J.J. (1988). "Single-layer models of evaporation from plant
798 canopies are incorrect but useful, whereas multilayer models are correct but useless'': discuss." *Aust J Plant Physiol*, 15, 705–716.

800 Rodriguez-Dominguez, C.M. & Brodribb, T.J. (2020). Declining root water transport drives
801 stomatal closure in olive under moderate water stress. *New Phytologist*, 225, 126–134.

802 Rosner, S., Heinze, B. & Savi, T. (2019). Prediction of hydraulic conductivity loss from
803 relative water loss : new insights into water storage of tree stems and branches, 843–854.

804 Ruel, J.J. & Ayres, M.P. (1999). Jensen's inequality predicts effects of environmental
805 variation. *Trends Ecol Evol*, 14, 361–366.

806 Sanchez-Martinez, P., Martínez-Vilalta, J., Dexter, K.G., Segovia, R.A. & Mencuccini, M.
807 (2020). Adaptation and coordinated evolution of plant hydraulic traits. *Ecol Lett*, 23,
808 1599–1610.

809 van der Sande, M.T., Zuidema, P.A. & Sterck, F. (2015). Explaining biomass growth of
810 tropical canopy trees: the importance of sapwood. *Oecologia*, 177, 1145–1155.

811 Scholz, F.G., Bucci, S.J., Goldstein, G., Meinzer, F.C., Franco, A.C. & Miralles-Wilhelm, F.
812 (2007). Biophysical properties and functional significance of stem water storage tissues
813 in Neotropical savanna trees. *Plant Cell Environ*, 30, 236–248.

814 Scholz, F.G., Phillips, N.G., Bucci, S.J., Meinzer, F.C. & Goldstein, G. (2011). Hydraulic
815 Capacitance: Biophysics and Functional Significance of Internal Water Sources in
816 Relation to Tree Size, 341–361.

817 Schrodinger, E. (1951). *What is life? The physical aspect of the living cell*. At the University
818 Press.

819 Spawn, S.A., Sullivan, C.C., Lark, T.J. & Gibbs, H.K. (2020). Harmonized global maps of
820 above and belowground biomass carbon density in the year 2010. *Sci Data*, 7, 1–22.

821 Sperry, J.S., Stiller, V. & Hacke, U.G. (2003). Xylem Hydraulics and the Soil–Plant–
822 Atmosphere Continuum: Opportunities and Unresolved Issues. *Agron J*, 95, 1362–1370.

823 Sperry, J.S., Venturas, M.D., Todd, H.N., Trugman, A.T., Anderegg, W.R.L., Wang, Y., *et*
824 *al.* (2019). The impact of rising CO 2 and acclimation on the response of US forests to
825 global warming, 116, 25734–25744.

826 Steudle, E. (2000). Water uptake by roots: Effects of water deficit. *J Exp Bot*, 51, 1531–1542.

827 Stewart, G.R., Gracia, C.A., Hegarty, E.E. & Specht, R.L. (1990). Nitrate reductase activity
828 and chlorophyll content in sun leaves of subtropical Australian closed-forest (rainforest)
829 and open-forest communities. *Oecologia*, 82, 544–551.

830 Tesař, M., Šír, M., Lichner, Ľ. & Čermák, J. (2007). Plant transpiration and net entropy
831 exchange on the Earth's surface in a Czech watershed. *Biologia (Bratisl)*, 62, 547–551.

832 Tyree, M. & Ewers, F. (1991). The hydraulic architecture of trees and other woody plants.
833 *New Phytologist*, 345–360.

834 Tyree, M.T. & Hammel, H. (1972). The measurement of the turgor pressure and the water
835 relations of plants by the pressure-bomb technique. *J Exp Bot*, 23, 267–282.

836 Tyree, M.T. & Sperry, J.S. (1989). Vulnerability of xylem to cavitation and embolism. *Annu.*
837 *Rev. Plant Phys. Mol. Bio*, 40, 19–38.

838 Venturas, M.D., Sperry, J.S. & Hacke, U.G. (2017). Plant xylem hydraulics: What we
839 understand, current research, and future challenges. *J Integr Plant Biol*, 59, 356–389.

840 Wang, X., Wang, C., Zhang, Q. & Quan, X. (2009). Heartwood and sapwood allometry of
841 seven Chinese temperate tree species. *Ann For Sci*, 67, 410–410.

842 Wolfe, B.T. & Kursar, T.A. (2015). Diverse patterns of stored water use among saplings in
843 seasonally dry tropical forests. *Oecologia*, 179, 925–936.

844 Wood, J.D., Gu, L., Hanson, P.J., Frankenberg, C. & Sack, L. (2023). The ecosystem wilting
845 point defines drought response and recovery of a Quercus-Carya forest. *Glob Chang*
846 *Biol*.

847 Yang, J., Medlyn, B.E., De Kauwe, M.G. & Duursma, R.A. (2018). Applying the Concept of
848 Ecohydrological Equilibrium to Predict Steady State Leaf Area Index. *J Adv Model*
849 *Earth Syst*, 10, 1740–1758.

850 Ziemińska, K., Rosa, E., Gleason, S.M. & Holbrook, N.M. (2020). Wood day capacitance is
851 related to water content, wood density, and anatomy across 30 temperate tree species.
852 *Plant Cell Environ*, 43, 3048–3067.

853

854

855

Figure legends

Figure 1. A schematic representing the distributions of water potential (Ψ), water storage (S), and biomass, throughout a forest profile. Panels A to C represent predawn non-drought (a); midday non-drought (b); and drought (c). The square boxes indicate 'representative' water potentials of the canopy and biomass in each scenario (where the colours relate to the water potential scale in the legend), i.e. the Ψ value of leaves at the top of the canopy, and a value intermediate between upper leaves and roots – these values converge at equilibrium. Panel (d) indicates the vertical profile of Ψ. Panel (e) represents the profile of water stored per ground area such that, for each horizontal slice (of 1 m vertical thickness), the water content is weighted by the biomass density given in (f) – note the different x axis applying to above and below ground fractions. Panel (f) shows a profile of the fractional cross sectional area of biomass ($m^2_{biomass}\ m^{-2}_{ground\ area}$) of a notional temperate forest. All gradients in Ψ are linear for simplicity (panel d), but this is unlikely to be representative of real conditions.

Figure 2. Panel a) shows a schematic relationship between water content (θ) and water potential (Ψ) of sapwood or leaves, generated using the following parameters: 1. Saturated water content, $\theta(\Psi_0)$; 2. Maximum water potential, Ψ_{max}; 3. Constant hydraulic capacitance throughout 'normal' physiological range indicated by the red double ended arrow, C; 4. Threshold water potential at which the PV relationship transitions into non-linear region, $\Psi_{threshold}$; 5. Exponentially declining capacitance as a function of water potential, $C_{post\text{-}threshold}$. Panel b) shows modelled relationships between the amount of water stored in the sapwood of individual trees (black lines, left axis) versus their equilibrium water potential in a simulated one hectare stand. The blue line in panel b) shows the total water stored in the above ground biomass (S_V, right axis) including the sum of all the sapwood water expressed per ground area, with respect to the equilibrium 'ecosystem water potential' (Ψ_E), blue line.

Figure 3. Ground area based vegetation water storage versus equilibrium water potential of the ecosystems described in Table S2: 1. Caxiuana (non-drought); 2. Caxiuana (artificially droughted); 3. Litchfield; 4. Tumbarumba; 5. Cow Bay; 6. Robson Creek; 7. Alice Mulga (semi-arid savanna); 8. Great Western Woodland;

9. Cumberland Plain. Each 'curve' is constructed from two lines, where the lower line represents the plot-level PV curve of the sapwood, and the upper line is the sum of the water content from sapwood and the canopy/leaf area; so, the difference between the curves, i.e., the line thickness, represents the canopy water content. The filled areas were constructed using data, while the hatched areas represent approximations of the pressure-volume relationship at water potentials below the water potential threshold. The points on each curve represent equilibrium water potentials as measured at predawn (blue), threshold, i.e. midday (red), and leaf turgor loss point (orange).

Figure 4. Relative water volume versus water potential of the sites described in Table 1. Each 'curve' is constructed from two lines, where the lower line represents the plot-level PV curve of the sapwood, and the upper line is the sum of the water content from sapwood and the canopy/leaf area; so the difference between the curves, i.e., the line thickness, represents the canopy water content. The filled areas were constructed using data, while the hatched areas represent approximations of the pressure-volume relationship following the water potential threshold for sapwood. The points on each curve represent equilibrium water potentials (Ψ) as measured at predawn (blue), threshold, i.e. midday (red), and leaf turgor loss point (orange).

Figure 5. Plot-level water relations parameters in relation to biomass expressed in absolute (a-c) and relative (d-e) terms. Hydraulic capacitance (a, d), accessible stored water between the maximum water potential and the threshold water potential (b, e), and the total amount of water stored in vegetation at saturation (c). Each number on the plot represents data from each site described in Table 1, where colours represent tropical rainforest (green), temperate forest (blue) and savanna (black): 1. Caxiuana (non-droughted); 2. Caxiuana (droughted); 3. Litchfield (wet trop. savanna); 4. Tumbarumba; 5. Cow Bay; 6. Robson Creek; 7. Alice Mulga (semi-arid savanna); 8. Great Western Woodland; 9. Cumberland Plain. Linear regressions are shown where the relationships are significant (a-c), and to reduce the number of significant figures the coefficients are multiplied by 10^3.

Figure 6. A comparison of the vegetation water storage (S_V) and plot equilibrium water potential of the drought plot (thick dashed line) and control plot (thick solid line) in the Caxiuana throughfall-exclusion experiment, based on data presented in Fig. 4. The red and blue points on each thick line represent the threshold water potential and measured predawn water potentials, respectively. The blue section of each line indicates the amount of water available in each plot for 'reversible' changes in ecosystem water content, i.e., changes that do not cause physiological damage. The red section of each of the thick lines represent a trajectory of water loss resulting in physiological damage and loss of living tissue/functional biomass. We hypothesise that the transition of the drought plot into its current reduced biomass state followed the red arrows to the point at which the biomass reached its current value given the available water. At that point, the equilibrium water potential would have returned to within the normal physiological range represented by the blue arrow (highlighted by the ellipse).

Figures

Figure 1

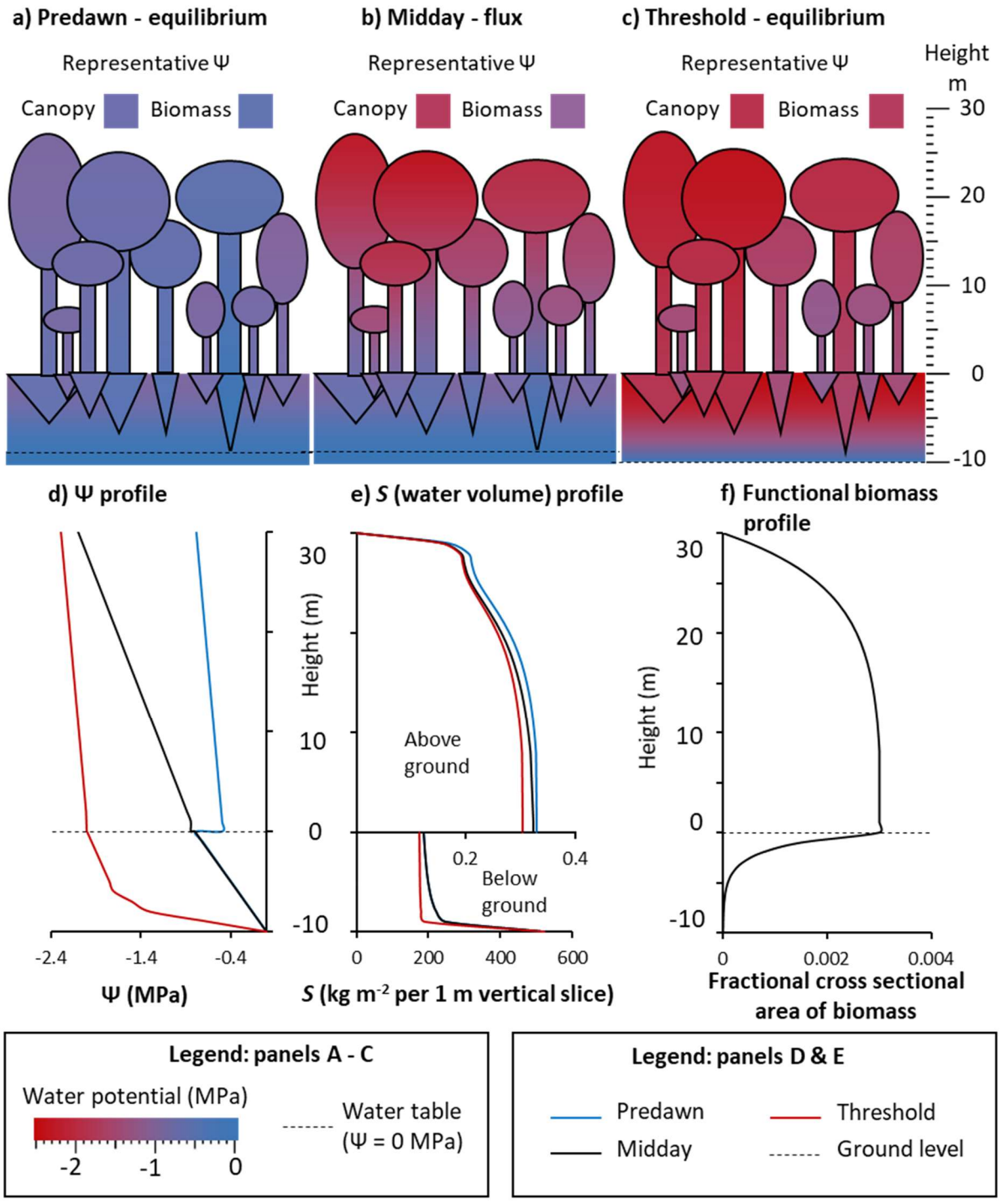

Figure 2

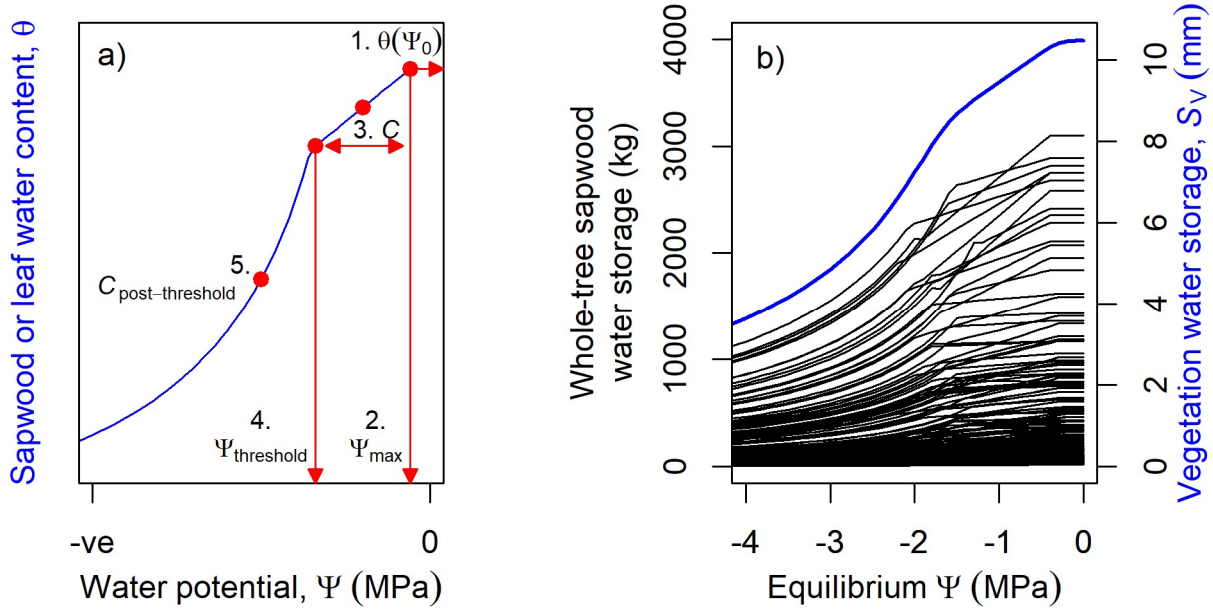

Figure 3

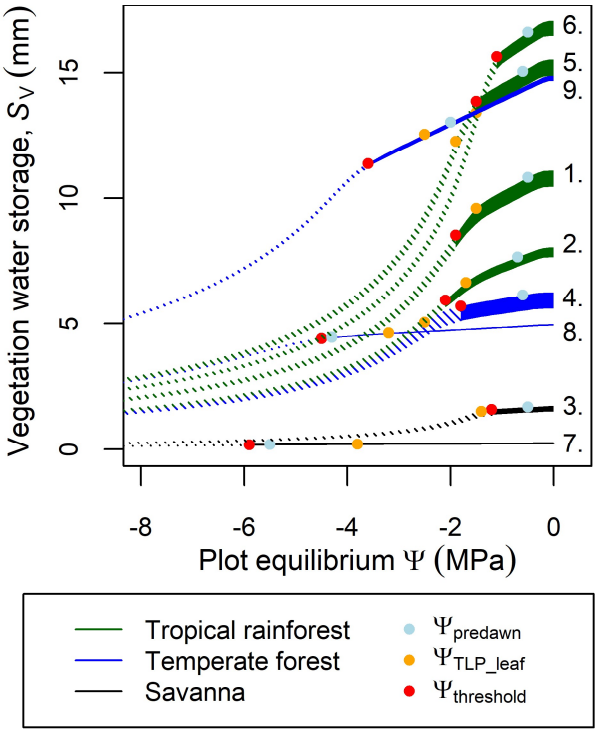

Figure 4

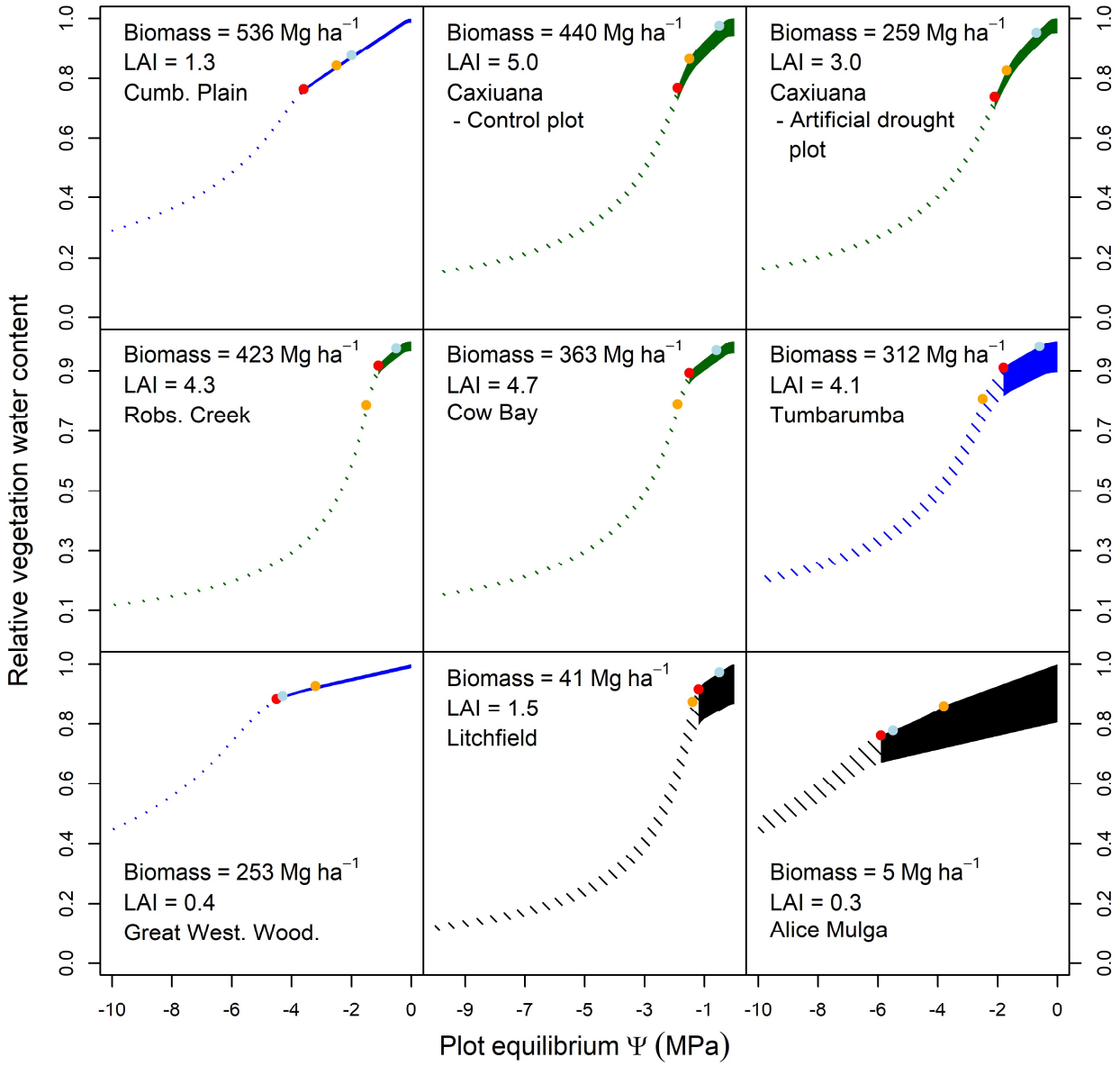
Biomass = 536 Mg ha^{-1}
LAI = 1.3
Cumb. Plain
Biomass = 440 Mg ha^{-1}
LAI = 5.0
Caxiuana
- Control plot
Biomass = 259 Mg ha^{-1}
LAI = 3.0
Caxiuana
- Artificial drought plot
Biomass = 423 Mg ha^{-1}
LAI = 4.3
Robs. Creek
Biomass = 363 Mg ha^{-1}
LAI = 4.7
Cow Bay
Biomass = 312 Mg ha^{-1}
LAI = 4.1
Tumbarumba
Biomass = 253 Mg ha^{-1}
LAI = 0.4
Great West. Wood.
Biomass = 41 Mg ha^{-1}
LAI = 1.5
Litchfield
Biomass = 5 Mg ha^{-1}
LAI = 0.3
Alice Mulga
Relative vegetation water content
Plot equilibrium Ψ (MPa)

Figure 5

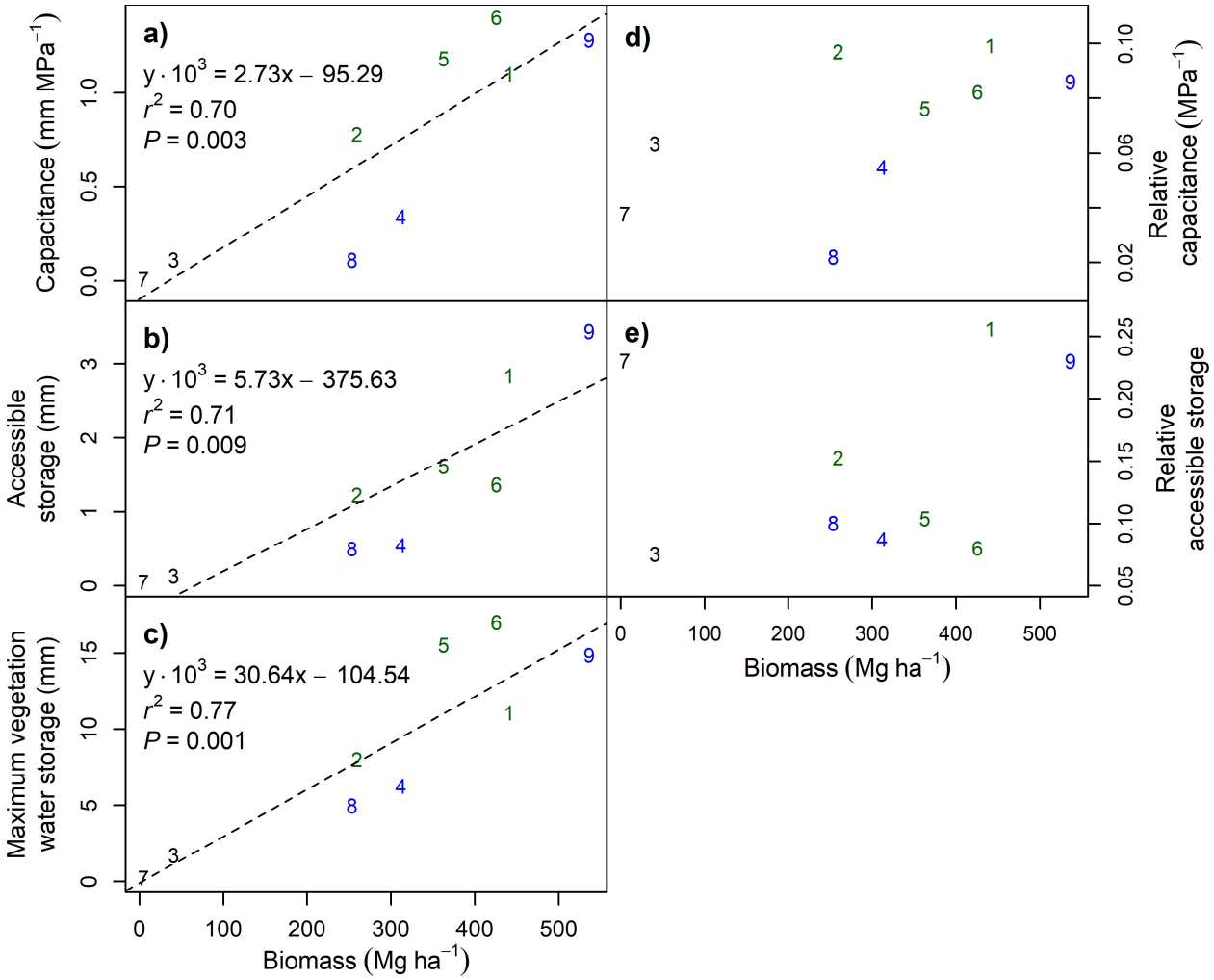
a)
y · 10^3 = 2.73x – 95.29
r^2 = 0.70
P = 0.003
b)
y · 10^3 = 5.73x – 375.63
r^2 = 0.71
P = 0.009
c)
y · 10^3 = 30.64x – 104.54
r^2 = 0.77
P = 0.001
d)
e)
Capacitance (mm MPa^-1)
Accessible storage (mm)
Maximum vegetation water storage (mm)
Relative capacitance (MPa^-1)
Relative accessible storage
Biomass (Mg ha^-1)
Biomass (Mg ha^-1)

Figure 6

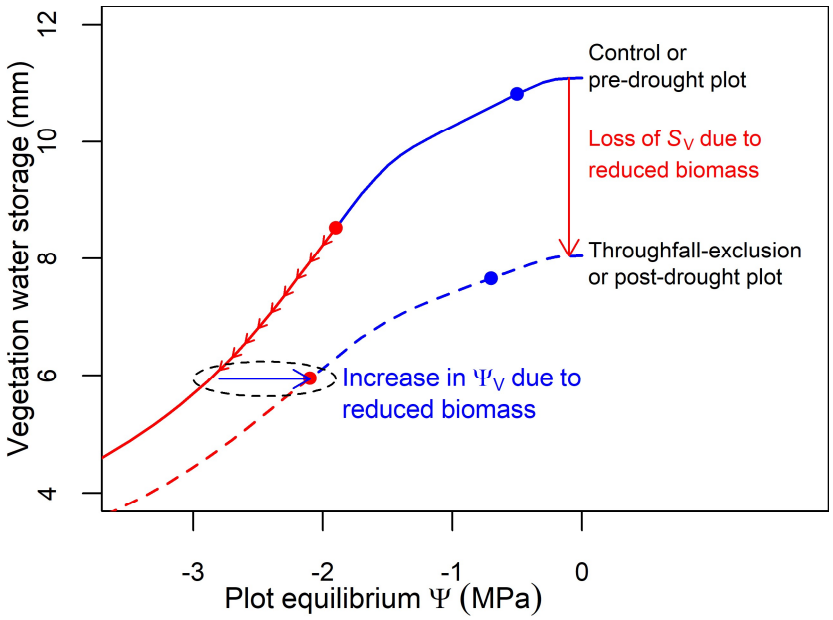
Vegetation water storage (mm)
4
6
8
10
12
-3
-2
-1
0
Plot equilibrium Ψ (MPa)
Control or
pre-drought plot
Loss of S_V due to
reduced biomass
Throughfall-exclusion
or post-drought plot
Increase in Ψ_V due to
reduced biomass

Tables

Table 1. Parameters used to derive the pressure-volume curves at the canopy- (plot-level averages), sapwood-, and plot-level.

Parameter (units)	Description	Derivation and/or references
		Canopy parameters
$\theta_{leaf}(\Psi_0)$ (kg $m^{-2}_{leaf\ area}$)	Leaf saturated water content	Derived from leaf mass per area (LMA) data as per Stewart et al., 1990, except for field site in Caxiuana, Brazil, which were measured by Binks et al., 2016. Plot mean LMA data from non-Caxiuana field sites were estimated from MODIS data (DAAC 2017).
$S_{canopy}(\Psi_i)$ (mm)	Canopy water	Total water contained in leaf area per ground area at Ψ_i. Equation 4.
LAI (m^2 m^{-2})	Leaf area index	Values taken from Beringer et al., 2016, except for field site in Caxiuana, Brazil, which were measured by Fisher et al., 2006.
C_{canopy} (mm MPa^{-1})	Canopy hydraulic capacitance	$C_{canopy} = \left(\frac{\mathrm{LAI} \cdot \theta_{leaf}(\Psi_0)\left[1 - \Theta_{leaf}(\Psi_{TLP})\right]}{-\Psi_{TLP}}\right)$
$\Theta_{leaf}(\Psi_{TLP})$ (unitless)	Leaf relative water content at turgor loss point	Biome-level values taken from Bartlett et al. 2012, except for field site in Caxiuana, Brazil, which were measured by Binks et al 2016
Ψ_{TLP} (MPa)	Leaf turgor loss point	Values taken from Bartlett et al. 2012, Binks et al. 2016, and Peters et al. 2021. See Table S3
		Sapwood parameters
Ψ_{max} (MPa)	Maximum (least negative) water potential	H_{tree} x -0.01, where H_{tree} is tree height (m), and -0.01 is a constant describing the gravitation effect on pressure (MPa m^{-1}) in a water column.
$\Psi_{predawn}$ (MPa)	Measured predawn canopy water potentials	See Table S1 for sources of data.
$\Psi_{threshold}$ (MPa)	Minimum safe water potential	This value is based on dry season midday leaf water potentials for the purpose of this analysis (See SI 4. *Choosing a threshold water potential*). Each tree was randomly allocated a value for $\Psi_{threshold}$ from a random normal distribution generated from the mean and standard deviation of midday leaf water potential values taken at a given site.
$\theta_{sw}(\Psi_0)$ (kg m^{-3})	Saturated sapwood water content	An empirical relationship reported by Dlouha et al. (2018) where $\Theta_{sat\_sw} = -0.67 \cdot \rho + 1$, and ρ is wood density.
$S_{sw\_plot}(\Psi_i)$ (mm)	Sapwood water	Total water contained in sapwood per ground area at Ψ_i. Equation 3.
C_{sw} (kg m^{-3} MPa^{-1})	Sapwood intensive capacitance of the linear phase of the pressure-volume curve.	Where field data exist, each tree was randomly allocated a value for C_1 from a random normal distribution generated from the mean and standard deviation of capacitance values. In the absence of field data, the mean value was derived from an empirical equation from Zieminska et al. (2020) of the form: $C_{sw} = -157.8 \cdot \rho + 137.7$, where ρ is wood density, and the standard deviation was taken as $0.5C_{sw}$.

V_{sw_tree} (m^3)	Volume of sapwood in a single tree	$V_{sw\_tree} = F_{sw} \cdot AGB_{tree}/\rho$
ρ_{wood} (kg m^{-3})	Wood density	Used to derive C_{sw}, Θ_{sat_sw}, and V_{AGB}. Obtained at species-level from plot inventories.
F_{sw} (dimensionless fraction)	Sapwood as a fraction of total volume	$F_{sw} = 2.9 \cdot DBH^{-0.6}$, derived as a compromise between the empirical relationship presented by Cordero & Kanninen (2003), and the ratio of sapwood area to basal area from Kunert et al. (2017), Moore et al. (2017), Aparecido et al. (2016) and Wang et al. (2009). See S2 for full details on deriving F_{sw}.
H_{tree} (m)	Tree height	Available in the datasets.
		Plot-level and other parameters
AGB (kg ha^{-1})	Above ground biomass	Taken from existing datasets
S_{soil} (mm)	Soil water	Total water contained in soil from the surface to depth D. Equation 2.
S_V (mm)	Vegetation water	Total water contained in vegetation per ground area at Ψ_i including canopy and sapwood components. $S_V = S_{canopy} + S_{sw}$
S_E (mm)	Ecosystem water content	Total water contained in ecosystem per ground area. Equation 1.
S_{V_a} (mm)	Accessible vegetation stored water	The difference in S_V between Ψ_{max} and the (equilibrium) threshold water potential, i.e., the theoretical maximum change in vegetation seasonal water storage.
C_V (mm MPa^{-1})	Vegetation hydraulic capacitance	The sum of the plot-level sapwood capacitance and the canopy capacitance. Equation 8.
$\boldsymbol{\rho}_{water}$ (kg m^{-3})	Water density	

Text boxes

Box 1 Intensive and extensive properties

"An intensive quantity is one whose magnitude is independent of the size of the system", for example pressure and temperature. Whereas "an extensive quantity is one whose magnitude is additive for subsystems", e.g., volume and mass (Mc Naught & Wilkinson, 2012, IUPAC Gold Book).

Plant physiologists and soil scientists commonly express quantities of water intensively by making water volume relative to a maximum value or by normalizing by the spatial extent of the system. This is a convenient way of isolating the properties of the system from the environment and provides insight into their internal structure and function. However, 'reconnecting' the system to the environment requires expressing quantities extensively such that a finite input/output results in a quantifiable change in the system. Thus, the intensive property θ ($m^3_{water}\ m^{-3}_{media}$) becomes an extensive volume of water S (m^3) when multiplied by the extensive volume of the system V (m^3).

Box 2 Equilibrium and Steady State

'Equilibrium' refers to the thermodynamic concept of a system at maximum entropy, where energy gradients have dissipated and there are no net fluxes. While evaporation is minimal, the system tends to a state in which the sum of water potential (Ψ) and gravitational potential at any point along the vertical profile is equal to the water potential of the source of water, i.e., there is no net gradient in the sum of energy potentials. Therefore, when transpiration is zero and the vegetation is at maximum possible hydration given the available soil water, the system is at equilibrium. This differs from 'steady-state', which refers to a constant gradient and/or constant flux.

PV curves of leaves (Tyree & Hammel 1972), water retention curves of soil (van Genuchten 1980), and moisture sorption isotherms of porous media (Franzen & Mirwald 2004) are all generated under equilibrium conditions, as gradients in water potential may result in mischaracterising the PV relationship. However, an equilibrium value for a given value of Ψ and water content (θ) may still be approximated in the presence of a Ψ gradient, providing the gradient and the material properties of the medium are sufficiently well characterised (e.g. **Fig. S1**). This could be achieved under steady-state conditions where the gradient is constant, or is changing slowly, over time. For example, it may be possible to know the relevant soil and canopy water potentials of a transpiring tree, but the Ψ and therefore θ at each point in the stem is unknown. In contrast, under 'equilibrium' conditions where the Ψ of the canopy and soil differ only by the difference in gravitational potential, the Ψ is known at each height in the stem, and the θ can be applied based on the known PV curve parameters.

Box 3 Summary of Water Potential in the Environment

Chemical processes, including phase changes and diffusion, progress towards an equilibrium state in which gradients in chemical potential are fully dissipated (Gibbs 1906). The hydrological cycle results from the continuous movement of water down a gradient of water potential towards an equilibrium state, and is perpetuated by the spatially and temporally variable input of energy across the Earth's surface (Kleidon & Schymanski 2008; Konings *et al.* 2012).

Following the pathway of water vertically upwards from its lowest point in a terrestrial system, we can define the water potential (Ψ) of the water table as 0 MPa, being free water at atmospheric pressure and assuming the osmotic potential is negligible. Above the water table, water is bound to the surface of soil particles and in pore spaces via capillarity, where the force of gravity, surface tension acting on menisci, and the resistance to the movement of water generates tension on the water column referred to as matric potential (negative hydrostatic pressure) (Hillel 1977). The relationship between water content of the soil and Ψ is determined by the pore size distribution whereby larger pores empty initially at pressures closer to 0 Pa, while the smallest pores can retain water at substantially lower pressures (Hollander 1979).

In plants, the relationship is more complex where adjacent tissues can maintain Ψ equilibrium by balancing osmotic potential and hydrostatic pressure. In the xylem and in cell walls, pressure is the dominant determinant of water potential (referred to as tension in xylem and matric potential in cell walls), and osmotic potential contributes minimally. In living tissues, water potential is determined by a combination of osmotic potential and turgor pressure (Pickard 1981).

The interface of the liquid-vapour phase change, in vegetation or soil, is typically the point of the system in which liquid water has its lowest chemical potential during evaporation. Evaporation and condensation are driven by the difference in chemical potential between the liquid and vapour (Ambaum 2020). The evaporation of water reduces the hydrostatic pressure, thus Ψ, of the evaporative surface, and the resulting gradient in Ψ is

transmitted through the vegetation and/or soil to the point at which Ψ is at its least negative value along the monotonic gradient of Ψ (Pickard 1981; Nobel 2009).

The atmospheric water potential oscillates diurnally according to temperature and humidity, typically achieving its lowest value (highest evaporative demand) around midday, and highest value at night during the formation of dew (when the gradient between the boundary layer and the liquid water surface is reversed) or during rainfall (Monteith & Unsworth 2013). Consequently, the temporal mean water potential (daily, seasonal, annual etc.) at the evaporative sites, occurs as a function of i) the magnitude, duration and dynamics of temporal changes in atmospheric potential; ii) the hydraulic conductance between the evaporative sites and the water source; iii) the pressure-volume relationship of the tissue between the evaporative sites and source; and iv) the Ψ of the source.